Supporting Information

for

Mechanisms and Kinetics of the Dehydrogenation of C_6-C_8 Cycloalkanes, Cycloalkenes, and Cyclodienes to Aromatics in H-MFI Zeolite Framework

Hansel Montalvo, Mykela DeLuca, Lauren Kilburn, and David Hibbitts*

[1]Department of Chemical Engineering, University of Florida, Gainesville, FL 32611, USA

*Corresponding author hibbitts@che.ufl.edu

Table of Contents

S1. ***Temperature Corrected Enthalpies, Entropies, and Gibbs Free Energies***

Enthalpies (*H*) and Gibb's free energies (*G*) can be calculated from density functional theory (DFT)-derived energies using statistical mechanics. Specifically, each is a sum of the electronic energy (E_0), the zero-point vibrational energy (ZPVE), and the respective vibrational, translational, and rotational motions of the species:

$$H = E_o + ZPVE + H_{vib} + H_{rot} + H_{trans} \tag{S1}$$

$$G = E_0 + ZPVE + G_{vib} + G_{rot} + G_{trans} \tag{S2}$$

at 623 K. Adsorbed species are not considered to have translational or rotational contributions; all such motions are modeled as frustrated vibrations on the zeolite pores. Vibrational, rotational, and translational enthalpies and free energies are estimated from other statistical mechanics formalisms:

$$ZPVE = \sum_i \left(\frac{1}{2} h\nu_i\right) \tag{S3}$$

$$H_{vib} = \sum_i \left(\frac{h\nu_i \exp\left(-\frac{h\nu_i}{kT}\right)}{1 - \exp\left(-\frac{h\nu_i}{kT}\right)} \right) \tag{S4}$$

$$G_{vib} = \sum_i \left(-kT \ln \left(\frac{1}{1 - \exp\left(-\frac{h\nu_i}{kT}\right)} \right) \right) \tag{S5}$$

$$H_{trans} = \frac{5}{2} kT \tag{S6}$$

$$H_{rot,linear} = kT \tag{S7}$$

$$H_{rot,nonlinear} = \frac{3}{2} kT \tag{S8}$$

$$G_{trans} = -kT \ln \left(\left(\frac{2\pi mkT}{h^2} \right)^{\frac{3}{2}} V \right) \tag{S9}$$

$$G_{rot} = -kT \ln \left(\frac{\pi^{\frac{1}{2}}}{\sigma} \left(\frac{T^3}{\theta_x \theta_y \theta_z} \right)^{\frac{1}{2}} \right) \tag{S10}$$

$$\theta_i = \frac{h^2}{8\pi^2 I_i k} \tag{S11}$$

where I_i is the moment of intertia about the *i* axis (either x, y, or z) and σ is the symmetry number of the species.[1]

S2. *Details of H-MFI Framework Structure and T-11*

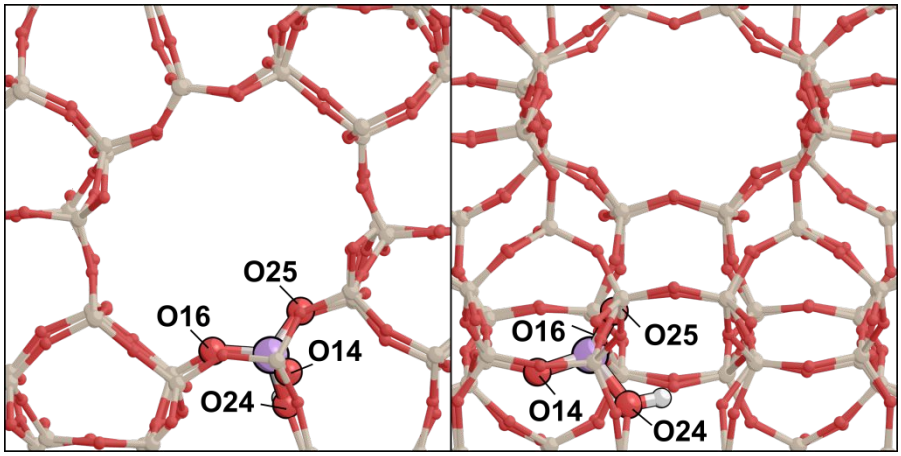

Figure S1. Straight (left) and sinusoidal (right) views of the H-ZSM-5 (MFI) structure.

S3. *Proton-mediated dehydrogenation of cyclohexane into benzene*

Figure S2 shows the sequential dehydrogenation of cyclohexane into benzene via proton-mediated routes, which is thermodynamically less favorable than the methyl-mediated route. Intrinsic activation barriers are 215, 164, and 141 kJ mol^{-1} for the dehydrogenation of C_6H_{12}, C_6H_{10}, and C_6H_8, respectively (623 K). Under the assumption that surface-bound methyls are the most-abundant surface intermediate (MASI), proton-mediated routes may not be as relevant as methyl-mediated routes. The unsteady-state character of MTO, however, may render proton-mediated routes relevant at low CH_3OH conversions, where surface-bound methyls are not MASI. Moreover, the kinetic relevance of proton- and methyl-mediated routes may be a function of catalyst bed length, where the relative distribution of surface-bound methyls and protons can change. A maximum rate analysis (Fig. 2d, main-text), however, suggests that at relative concentrations of proton-to-methyl as high 10^4, methyl-mediated routes will govern the dehydrogenation of C_6 hydrocarbon rings.

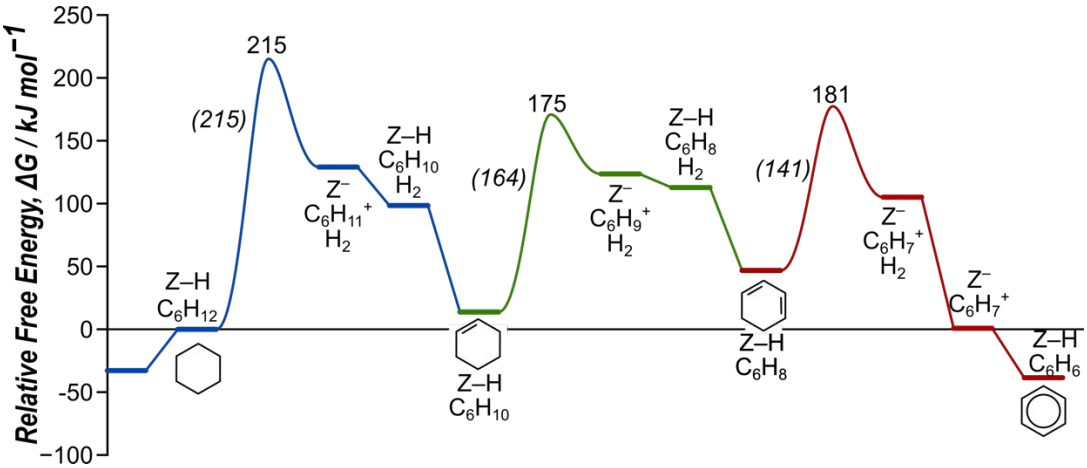

Figure S2. Reaction coordinate diagram for the sequential proton-mediated dehydrogenation of cyclohexane into benzene. Dehydrogenation reactions are shown for C_6H_{12} (blue), C_6H_{10} (green), and C_6H_8 (red). Free energy barriers (ΔG in kJ mol^{-1}) are reported at 623 K and referenced to cyclohexane adsorbed near a proton.

S4. ***Maximum Rate Analysis of Dehydrogenation Reactions***

Maximum rate analysis is used here to identify the maximum rate of reaction (assuming all prior steps are quasi equilibrated) if a given elementary step is rate-determining. For a given dehydrogenation reaction, the hydride transfer step was found to be rate-determining. For the sequential dehydrogenation of cycloalkanes into aromatics, however, there are three sequential hydride transfers; maximum rate analysis is used to determine which of the three is rate-limiting.

The rate expressions for these potential rate-limiting steps via proton-mediated dehydrogenation are:

$$r_{\mathrm{C6H12}} = k_{\mathrm{H\,-\,Z\,-\,C6H12,app}}\,[\mathrm{Z{-}H}]\;P_{C6H12} \qquad \text{(Eq. S1)}$$

$$r_{\mathrm{C6H10}} = k_{\mathrm{H\,-\,Z\,-\,C6H10,app}}\,[\mathrm{Z{-}H}]\;P_{C6H12}P_{H2}^{-1} \qquad \text{(Eq. S2)}$$

$$r_{\mathrm{C6H8}} = k_{\mathrm{H\,-\,Z\,-\,C6H8,app}}\,[\mathrm{Z{-}H}]\;P_{C6H12}P_{H2}^{-2} \qquad \text{(Eq. S3)}$$

where $k_{\mathrm{H\,-\,Z\,-\,C6H12,app}}$, $k_{\mathrm{H\,-\,Z\,-\,C6H10,app}}$, and $k_{\mathrm{H\,-\,Z\,-\,C6H8,app}}$ are the apparent rate coefficients for the proton-mediated dehydrogenation of cyclohexane, cyclohexene, and cyclohexadiene respectively, [H–Z] is the concentration of bare protons, and P_{C6H12} and P_{H2} are the gas phase pressures of cyclohexane and molecular hydrogen, respectively.

Equations S1-S3 are referenced to gas phase cyclohexane to explore the sequential dehydrogenation from cyclohexane into benzene. These rate expressions differ in hydrogen pressure (P_{H2}) order dependencies, reflecting the corresponding hydrogen formation from preceding dehydrogenations (e.g., two dehydrogenations precede the formation of cyclohexadiene from cyclohexane, therefore, its dehydrogenation rate into benzene is proportional to P_{H2}^{-2}).

Figure S3 shows the ratio between Equation S2 (green) and Equation S3 (red) relative to Equation S1, both as a function of temperature and gas-phase hydrogen pressure. While varying temperature allows for probing the role of thermodynamics on rate limiting steps, varying hydrogen pressures serves as a proxy for conversion (i.e., higher H_2 pressures represent higher conversions). Rate ratio values above unity indicate that the rate from the denominator is rate-limiting, while the opposite holds true for rate ratio values below unity.

Values for the ratio of cyclohexene dehydrogenation to cyclohexane dehydrogenation are always above unity, suggesting that cyclohexane dehydrogenation is always rate-limiting in the range of reported temperatures (333-1000 K) as well as in the range of reported H_2 pressures (10^{-2}-10^{2} bar).

In the case of the ratio of cyclohexadiene dehydrogenation to cyclohexane dehydrogenation, however, there is a shift in rate-limiting step from cyclohexane dehydrogenation at high temperatures (500-1000 K) to cyclohexadiene dehydrogenation at lower temperatures (333-500

K). Rate ratio values suggest that entropy gains associated with the formation and subsequent desorption of molecular H_2 favor cyclohexadiene dehydrogenation over cyclohexane dehydrogenation (2 moles of H_2 precede cyclohexadiene dehydrogenation) at relatively high temperatures.

A shift from cyclohexane dehydrogenation to cyclohexadiene dehydrogenation as rate-limiting step is also reported at relatively high H_2 pressures (10^1-10^2 bar H_2). This suggests that the differences in H_2 formation preceding the dehydrogenation of cyclohexadiene will diminish the rate of cyclohexadiene dehydrogenation at relatively high H_2 pressures (i.e., high conversion) to a greater extent than that of the rate of cyclohexane dehydrogenation. Barriers for proton-mediated dehydrogenation are never lower than that of methyl-mediated routes, therefore, the conclusions derived from maximum rate analysis of proton-mediated routes will only be relevant at very low methanol conversion (i.e., Z–CH_3 low coverage).

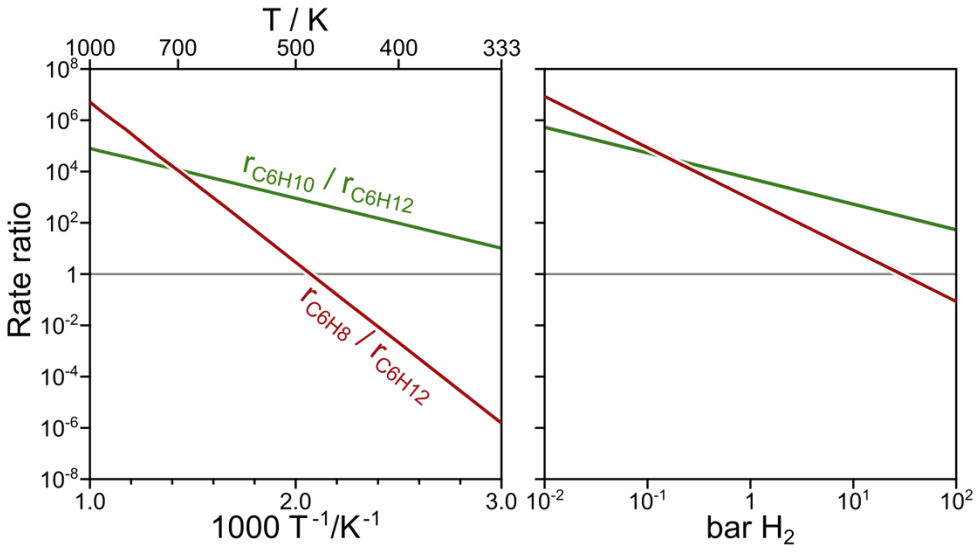

Figure S3. Ratio of rates for proton-mediated dehydrogenation of cyclohexene (green) and cyclohexadiene (red) to proton mediated dehydrogenation of cyclohexane as a function of temperature (left, (H_2) = 1bar) and gas phase product H_2 pressure (right, 623 K).

For the case of the methyl-mediated dehydrogenation, the corresponding expressions for the rate-limiting steps are:

$$r_{C6H12} = k_{CH3\text{-}Z\text{-}C6H12,app}\,[Z\text{–}H]\,P_{C6H12}P_{ROCH3}P_{ROH}^{-1} \quad \text{(Eq. S4)}$$

$$r_{C6H10} = k_{CH3\text{-}Z\text{-}C6H10,app}\,[Z\text{–}H]\,P_{C6H12}P_{ROCH3}^{2}P_{ROH}^{-2}P_{CH4} \quad \text{(Eq. S5)}$$

$$r_{C6H8} = k_{CH3\text{-}Z\text{-}C6H8,app}\,[Z\text{–}H]\,P_{C6H12}P_{ROCH3}^{3}P_{ROH}^{-3}P_{CH4}^{2} \quad \text{(Eq. S6)}$$

where $k_{CH3\text{-}Z\text{-}C6H12,app}$, $k_{CH3\text{-}Z\text{-}C6H10,app}$, and $k_{CH3\text{-}Z\text{-}C6H8,app}$ are the apparent rate coefficients for the methyl-mediated dehydrogenation of cyclohexane, cyclohexene, and cyclohexadiene respectively, and P_{C6H12}, P_{CH4}, P_{ROCH3}, and P_{ROH} are the gas-phase pressures of cyclohexane,

methane, methyl-source (methanol or dimethyl-ether), and the corresponding gas-phase surface-methylation product (water or methanol, Rxn. 3).

These expressions are referenced to gas-phase cyclohexane to capture the sequential dehydrogenation from cyclohexane into benzene. Surface bound-methyls are formed from surface-methylation reactions (Rxn. 3) which consumes and produces a $ROCH_3$ and ROH species respectively. Hence, rate expressions will depend on these accordingly, and their order reflects the number of preceding surface-methylation steps before dehydrogenation. Methane, the corresponding product upon methyl-mediated dehydrogenation, is analogous to H_2 in proton-mediated routes. As such, rate expressions will also depend on CH_4 gas-phase pressure, and its order reflects the number of preceding stoichiometrically formed CH_4 before dehydrogenation.

Figure S4 shows the corresponding rate ratio between Equation S5 (green) and Equation S6 (red) to Equation S4 as both a function of temperature and corresponding gas phase pressures. Again, the ratio of gas phase pressures serves as a proxy for conversion (i.e., higher values of gas phase reactants to products indicate lower conversions). Figure S4 shows that the value of the rate ratio as a function of both temperature and pressure is always above unity, suggesting that cyclohexane dehydrogenation is always the rate-limiting step. As such, we conclude that, for a given series of methyl-mediated dehydrogenation events, the very first hydride transfer will always be rate-limiting.

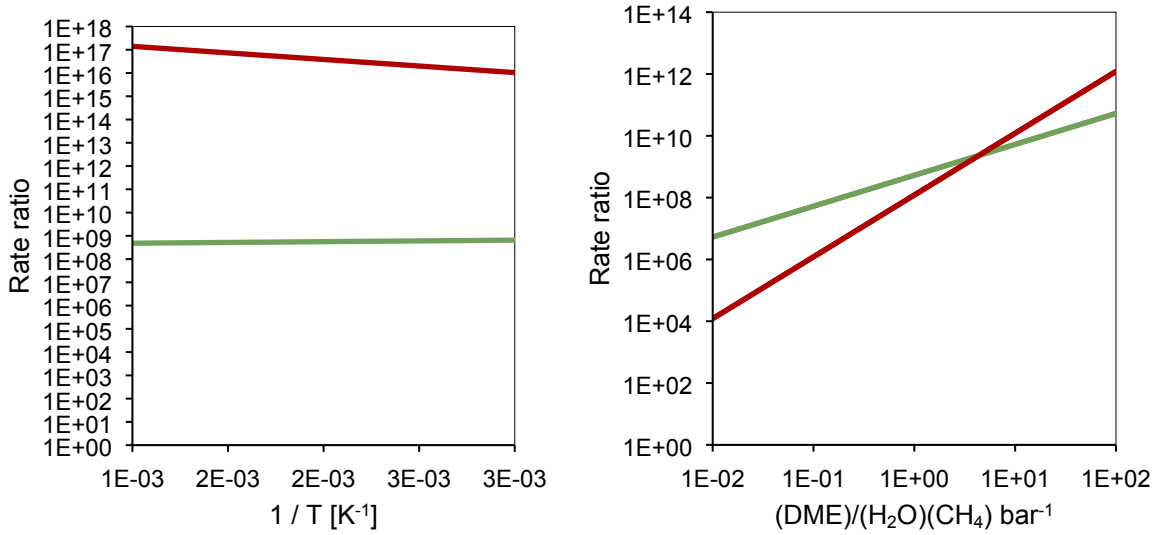

Figure S4. Ratio of rates for methyl-mediated dehydrogenation of cyclohexene (green) and cyclohexadiene (red) to methyl-mediated dehydrogenation of cyclohexane as a function of temperature (left, $(CH_3OCH_3)=(CH_4)=(H_2O)=1$bar) and relative pressures of gas phase reactants to products (right, 623 K).

S5. *Gas phase formation of C_6-C_8 carbocations*

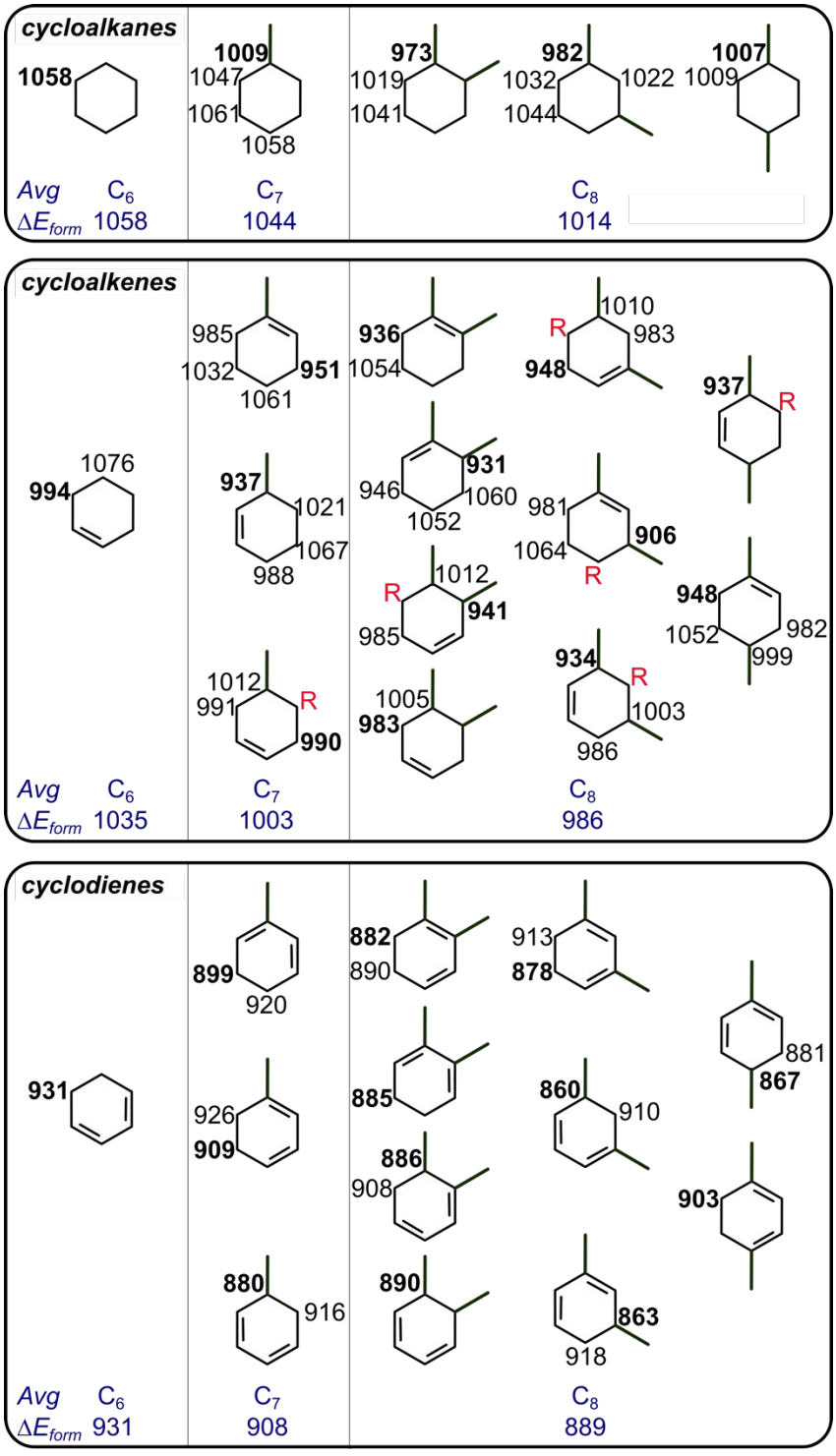

Figure S5. Gas phase carbocation formation energies for cycloalkanes, cycloalkenes, and cyclodienes. Formation energies (ΔE kJ mol^{-1}) are balanced with gas phase energy of hydride anion (H^-) and are shown next to the Carbon-atom participating in the C–H heterolytic activation. Carbocations that undergo restructuring are shown with R in red.

Carbocation stabilities, in part, determine the location at which a hydride transfer—and thus, the carbocation ring that is formed—events occur. The gas phase formation of C_6–C_8 carbocations was investigated as a function of hydride transfer location, relative to methyl-substituents, to assess the role of methyl-substituents present on hydrocarbon rings on methyl-mediated dehydrogenation activation barriers. Carbocation formation energies were estimated as follows:

$$E_{form} = E_{carbocation} + E_{hydride} - E_{ring} \quad \text{(Eq. S7)}$$

from estimated energies of gas phase carbocation, a hydride anion, and hydrocarbon ring, respectively. Fig. S5 shows the corresponding carbocation formation energies at the location of hydride transfer. These data suggest that the presence of methyl-substituents lowers carbocation formation energies, as averaged values decrease from C_6 to C_8 carbocations. Moreover, for a given ring, carbocations formed from hydride transfers occurring near methyl-substituents have lower carbocation formation energies.

Fig. S6 shows gas-phase carbocation formation energies as a function of their corresponding methyl-mediated hydride transfer. There is a no correlation between these two descriptors, suggesting that the carbocation formation trends are not transferable to ring dehydrogenation routes. This is likely because of the convolution of steric-hindrances, arising from interactions between methyl-substituents and hydride acceptor species, which increase barriers and the relative confinement effects from zeolite frameworks which can serve to decrease barriers (if appropriately solvated). To surmise, ring dehydrogenation is governed by a convolution of carbocation stabilities, sterics, and confinement effects and additional methyl substituents serve to increase hydride transfer barriers (Fig. 5, main text).

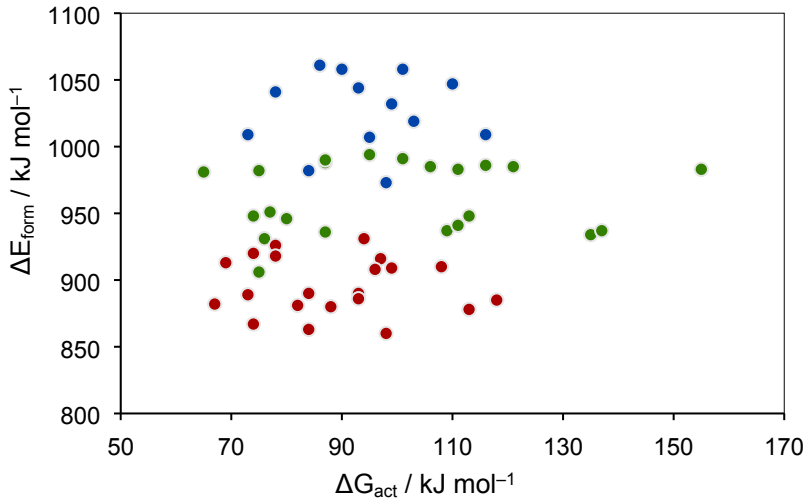

Figure S6. Gas phase carbocation formation energies for cycloalkanes (blue), cycloalkenes (green), and cyclohexadiene (red) as a function of their corresponding methyl-mediated hydride transfer activation barriers, referenced to ring coadsorbed near a CH_3–Z. Carbocation formation energies and activation barriers are reported at 623 K.

S7. ***Reaction coordinate diagrams for ortho-, meta-, and para-xylene formation***

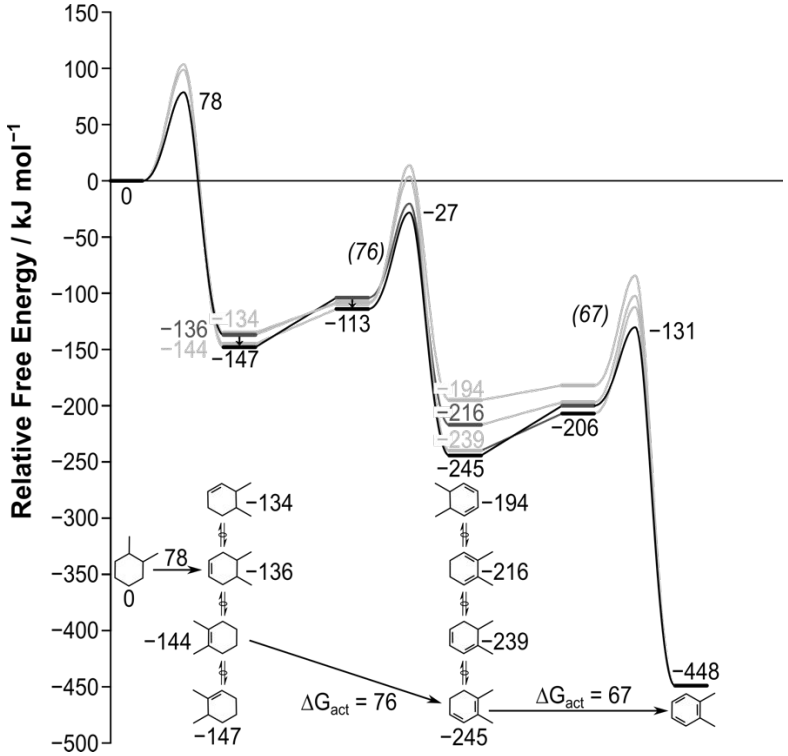

Figure S7. Reaction coordinate diagram for the dehydrogenation of 1,2-dimethyl-cyclohexane into ortho-xylene. Lowest energy path is shown in black. Free energies are reported relative to corresponding cycloalkane near a surface-bound methyl and at 623 K.

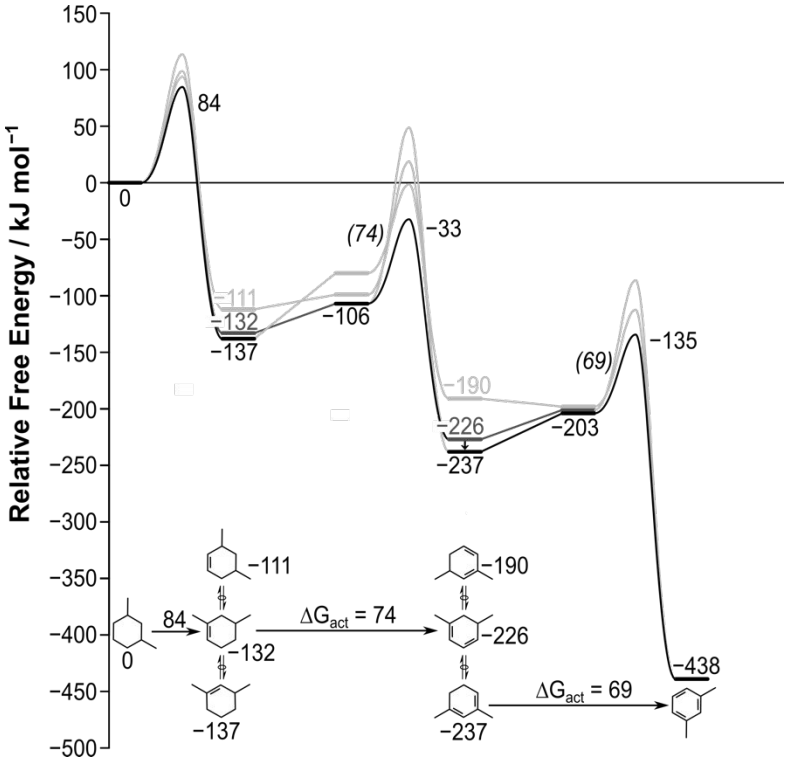

Figure S8. Reaction coordinate diagram for the dehydrogenation of 1,3-dimethyl-cyclohexane into meta-xylene. Lowest energy path is shown in black. Free energies are reported relative to corresponding cycloalkane near a surface-bound methyl and at 623 K.

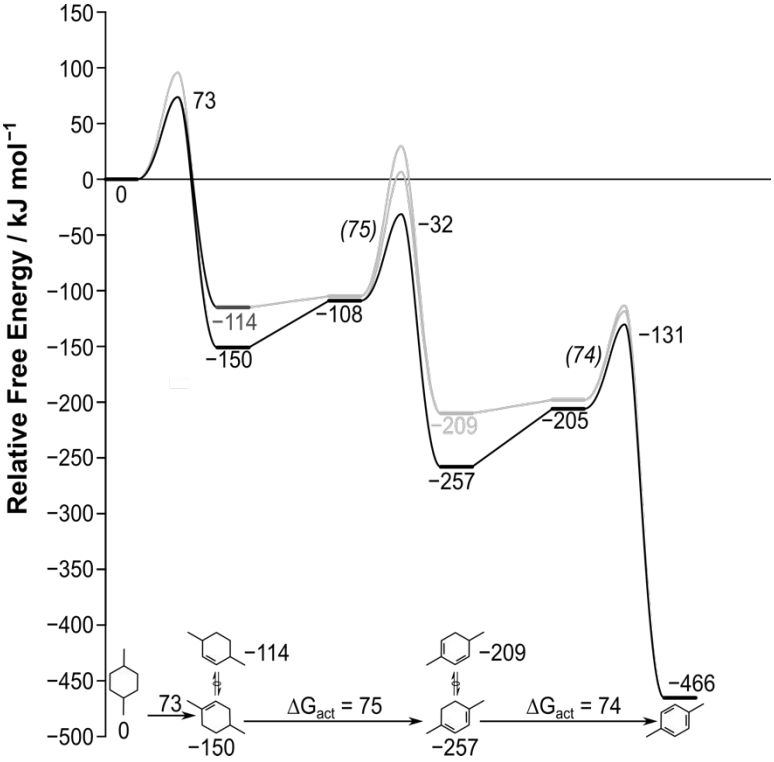

Figure S9. Reaction coordinate diagram for the dehydrogenation of 1,4-dimethyl-cyclohexane into para-xylene. Lowest energy path is shown in black. Free energies are reported relative to corresponding cycloalkane near a surface-bound methyl and at 623 K.

Methyl-substituents generally hinder the hydride transfer reactions at geminal and ortho positions relative to the substituent, as discussed for C_7 rings in main text. Similarly, the presence of two-methyl substituents in C_8 rings governs hydride transfer locations as these occur with lower activation barriers away from substituents. Double-bond isomerization facilitates aromatization toward xylenes formation, as the quasi-equilibrated conversion between these allow then for hydride transfers to occur away from methyl-substituents. The conclusions discussed for C_7 are thus extendible for C_8 hydrocarbon rings, suggesting that the dehydrogenation of methylated cyclization products may also contribute to the formation of xylenes during MTO chemistry, which pronounces the relevance of these reactions in governing the relative distribution of MTO products. Like C_7 estimates, here we considered all double-bond isomers for each C_8 skeletal isomer. Overall, aromatization proceeds from most stable double-bond isomers, which were found to be activated with the lowest activation energies.

S8. *Energies of Reactant, Product, and Transition State Structures*

Table S1. Energies of Transition States at 623K in H-ZSM-5 (MFI) Referenced to Best Overall Reactant as a Function of Zeolite Environment.

		Intersection			Straight Channel			
		ΔH≠	**ΔG≠**	**ΔS≠**	**ΔH≠**	**ΔG≠**	**ΔS≠**	
O-atom	**Reaction**	kJ mol^{-1}	kJ mol^{-1}	J K^{-1} mol^{-1}	kJ mol^{-1}	kJ mol^{-1}	J K^{-1} mol^{-1}	Structure
		Proton-mediated Dehydrogenation						
O16	*Ref*: Z–H + C_6H_x*	0	0	0	0	0	0	
O14	$C_6H_{12} \rightarrow C_6H_{11}^+$	191	193	–4	246	251	–7	S10 (a),(d)
O14	$C_6H_{10} \rightarrow C_6H_9^+$	181	190	–15	257	261	–6	S12 (a),(d)
O14	$C_6H_8 \rightarrow C_6H_7^+$	145	160	–24	162	177	–25	S14 (a),(d)
O16	$C_6H_{12} \rightarrow C_6H_{11}^+$	212	200	19	220	223	–5	S10 (b),(e)
O16	$C_6H_{10} \rightarrow C_6H_9^+$	175	178	–4	189	195	–10	S12 (b),(e)
O16	$C_6H_8 \rightarrow C_6H_7^+$	131	138	–12	158	174	–26	S14 (b),(e)
O25	$C_6H_{12} \rightarrow C_6H_{11}^+$	198	207	–14	200	205	–7	S10 (c),(f)
O25	$C_6H_{10} \rightarrow C_6H_9^+$	232	224	13	235	228	10	S12 (c),(f)
O25	$C_6H_8 \rightarrow C_6H_7^+$	125	129	–7	133	144	–18	S14 (c),(f)
		Methyl-mediated Dehydrogenation						
O16	*Ref*: Z–CH_3 + C_6H_x*	0	0	0	0	0	0	
O14	$C_6H_{12} \rightarrow C_6H_{11}^+$	119	137	–29	197	224	–43	S11 (a),(d)
O14	$C_6H_{10} \rightarrow C_6H_9^+$	109	128	–37	170	197	–44	S13 (a),(d)
O14	$C_6H_8 \rightarrow C_6H_7^+$	110	130	–32	161	189	–45	S15 (a),(d)
O16	$C_6H_{12} \rightarrow C_6H_{11}^+$	100	110	–16	158	184	–42	S11 (b),(e)
O16	$C_6H_{10} \rightarrow C_6H_9^+$	77	93	–26	150	178	–45	S13 (b),(e)
O16	$C_6H_8 \rightarrow C_6H_7^+$	69	88	–31	168	198	–49	S15 (b),(e)
O25	$C_6H_{12} \rightarrow C_6H_{11}^+$	167	193	–41	167	193	–41	S11 (c),(f)
O25	$C_6H_{10} \rightarrow C_6H_9^+$	86	102	–25	149	178	–46	S13 (c),(f)
O25	$C_6H_8 \rightarrow C_6H_7^+$	69	90	–34	132	162	–49	S15 (c),(f)

Table S2. Energies of States in H-ZSM-5 (MFI) for the methyl-mediated conversion of cyclohexane into benzene.

State	ΔH kJ mol^{-1}	ΔG kJ mol^{-1}	ΔS J K^{-1} mol^{-1}
Z–CH_3 + C_6H_{12}*	0	0	0
[C_6H_{12}--CH_3--Z]≠	19	90	4
Z^- + $C_6H_{11}^+$ + CH_4*	99	-22	-13
Z^- + $C_6H_{11}^+$	32	-56	59
Z–H + C_6H_{10}*	59	-139	156
Z–CH_3 + C_6H_{10}*	-25	-123	156
[C_6H_{10}--CH_3--Z]≠	-5	-28	162
Z^- + $C_6H_9^+$ + CH_4*	77	-161	140
Z^- + $C_6H_9^+$	-8	-202	217
Z–H + C_6H_8*	13	-237	319
Z–CH_3 + C_6H_8*	-21	-219	319
[C_6H_8--CH_3--Z]≠	0	-138	325
Z^- + $C_6H_7^+$ + CH_4*	67	-295	302
Z–H + C_6H_6*	-72	-456	331

Table S3. Energies of Transition States for C_6-C_8 cycloalkanes, cycloalkenes, and cyclodienes at 623K in H-ZSM-5 (MFI)

Reaction	HT-position	**ΔH≠** kJ mol^{-1}	**ΔG≠** kJ mol^{-1}	**ΔS≠** J K^{-1} mol^{-1}	
Ref: Z–CH_3 + C_mH_n*	--	0	0	0	Structure
Cycloalkanes					
$C_6H_{12} \rightarrow C_6H_{11}^+$	--	100	110	–16	S11 (b)
$C_7H_{14} \rightarrow C_7H_{13}^+$	*geminal*	99	116	-27	S18 (c)
$C_7H_{14} \rightarrow C_7H_{13}^+$	*ortho*	93	110	-27	S18 (a)
$C_7H_{14} \rightarrow C_7H_{13}^+$	*meta*	72	86	-23	S18 (b)
$C_7H_{14} \rightarrow C_7H_{13}^+$	*para*	78	90	-20	S18 (d)
o-$C_8H_{16} \rightarrow C_8H_{15}^+$	*gem-ortho*	83	98	-24	S19 (a)
o-$C_8H_{16} \rightarrow C_8H_{15}^+$	*ortho-meta*	84	103	-30	S19 (b)
o-$C_8H_{16} \rightarrow C_8H_{15}^+$	*meta-para*	67	78	-18	S19 (c)
m-$C_8H_{16} \rightarrow C_8H_{15}^+$	*gem-meta*	68	84	-27	S19 (d)
m-$C_8H_{16} \rightarrow C_8H_{15}^+$	*ortho-para*	79	99	-32	S19 (e)
m-$C_8H_{16} \rightarrow C_8H_{15}^+$	*meta-meta*	73	93	-31	S19 (f)
m-$C_8H_{16} \rightarrow C_8H_{15}^+$	*ortho-ortho*	92	113	-34	S19 (g)
p-$C_8H_{16} \rightarrow C_8H_{15}^+$	*gem-para*	64	73	-14	S19 (h)
p-$C_8H_{16} \rightarrow C_8H_{15}^+$	*ortho-meta*	87	95	-11	S19 (i)
Cycloalkenes					
$C_6H_{10} \rightarrow C_6H_9^+$	--	82	95	-22	S13 (b)
1-$C_7H_{12} \rightarrow C_7H_{11}^+$	*ortho*	91	106	-24	S18 (f)
1-$C_7H_{12} \rightarrow C_7H_{11}^+$	*meta*	58	77	-30	S18 (e)
3-$C_7H_{12} \rightarrow C_7H_{11}^+$	*geminal*	90	109	-31	S18 (g)
3-$C_7H_{12} \rightarrow C_7H_{11}^+$	*para*	66	87	-33	S18 (h)
4-$C_7H_{12} \rightarrow C_7H_{11}^+$	*ortho*	80	101	-34	S18 (i)
4-$C_7H_{12} \rightarrow C_7H_{11}^+$	*meta*	72	87	-24	S18 (j)
1,2-$C_8H_{14} \rightarrow C_7H_{13}^+$	*ortho-meta*	70	87	-27	S20 (a)
1,6-$C_8H_{14} \rightarrow C_7H_{13}^+$	*meta-para*	69	80	-17	S20 (b)
1,6-$C_8H_{14} \rightarrow C_7H_{13}^+$	*gem-ortho*	72	76	-6	S20 (c)
3,4-$C_8H_{14} \rightarrow C_7H_{13}^+$	*meta-para*	99	121	-36	S20 (d)
3,4-$C_8H_{14} \rightarrow C_7H_{13}^+$	*gem-ortho*	91	111	-33	S20 (e)
4,5-$C_8H_{14} \rightarrow C_7H_{13}^+$	*ortho-meta*	87	111	-38	S20 (f)
1,5-$C_8H_{14} \rightarrow C_7H_{13}^+$	*meta-meta*	57	74	-26	S20 (g)
1,5-$C_8H_{14} \rightarrow C_7H_{13}^+$	*ortho-ortho*	139	155	-26	S20 (h)
1,3-$C_8H_{14} \rightarrow C_7H_{13}^+$	*ortho-para*	50	65	-25	S20 (i)
1,3-$C_8H_{14} \rightarrow C_7H_{13}^+$	*gem-meta*	60	75	-24	S20 (j)
3,5-$C_8H_{14} \rightarrow C_7H_{13}^+$	*gem-meta*	110	135	-39	S20 (k)
3,5-$C_8H_{14} \rightarrow C_7H_{13}^+$	*ortho-para*	92	116	-39	S20 (l)
3,6-$C_8H_{14} \rightarrow C_7H_{13}^+$	*gem-para*	115	137	-35	S20 (m)
1,4-$C_8H_{14} \rightarrow C_7H_{13}^+$	*ortho-meta*	99	113	-23	S20 (n)
1,4-$C_8H_{14} \rightarrow C_7H_{13}^+$	*ortho-meta*	60	75	-24	S20 (o)
Cyclodienes					
$C_6H_8 \rightarrow C_6H_7^+$	--	67	81	-23	S15 (b)
2-$C_7H_{10} \rightarrow C_7H_9^+$	*meta*	69	84	-24	S18 (l)
1-$C_7H_{10} \rightarrow C_7H_9^+$	*ortho*	59	74	-24	S18 (k)
4-$C_7H_{10} \rightarrow C_7H_9^+$	*ortho*	69	88	-24	S18 (m)
1,2-$C_8H_{12} \rightarrow C_8H_{11}^+$	*ortho-meta*	78	97	-30	S21 (a)
1,2-$C_8H_{12} \rightarrow C_8H_{11}^+$	*meta-para*	57	67	-16	S21 (b)
2,3-$C_8H_{12} \rightarrow C_8H_{11}^+$	*meta-para*	82	93	-18	S21 (c)
1,6-$C_8H_{12} \rightarrow C_8H_{11}^+$	*gem-ortho*	104	118	-22	S21 (d)
1,6-$C_8H_{12} \rightarrow C_8H_{11}^+$	*ortho-meta*	81	93	-19	S21 (e)
5,6-$C_8H_{12} \rightarrow C_8H_{11}^+$	*gem-ortho*	85	96	-18	S21 (f)
1,3-$C_8H_{12} \rightarrow C_8H_{11}^+$	*ortho-meta*	71	84	-21	S21 (g)

1,3-C_8H_{12} → $C_8H_{11}^+$	*meta-meta*	53	69	-25	S21 (h)
1,5-C_8H_{12} → $C_8H_{11}^+$	*gem-meta*	93	113	-33	S21 (i)
1,5-C_8H_{12} → $C_8H_{11}^+$	*ortho-ortho*	82	98	-25	S21 (j)
3,5-C_8H_{12} → $C_8H_{11}^+$	*ortho-para*	68	84	-25	S21 (k)
3,5-C_8H_{12} → $C_8H_{11}^+$	*gem-meta*	88	108	-32	S21 (l)
2,5-C_8H_{12} → $C_8H_{11}^+$	*gem-para*	77	82	-8	S21 (m)
2,5-C_8H_{12} → $C_8H_{11}^+$	*ortho-meta*	71	83	-20	S21 (n)
1,4-C_8H_{12} → $C_8H_{11}^+$	*ortho-meta*	65	74	-14	S21 (o)

Table S4. Energies of States in H-ZSM-5 (MFI) for the methyl-mediated conversion of methyl-cyclohexane into toluene

State	ΔH kJ mol^{-1}	ΔG kJ mol^{-1}	ΔS J K^{-1} mol^{-1}	Structure
Z–CH_3 + C_7H_{14}*	0	0	0	S17 (a)
[1p-1-C_7H_{13}--H--CH_3--Z]≠	93	110	-27	S18 (a)
[1p-4-C_7H_{13}--H--CH_3--Z]≠	72	86	-23	S18 (b)
[1p-2-C_7H_{13}--H--CH_3--Z]≠	99	116	-27	S18 (c)
[1p-5-C_7H_{13}--H--CH_3--Z]≠	78	90	-20	S18 (d)
Z–H + 1-C_7H_{12}*	-72	-114	135	S17 (b)
Z–H + 3-C_7H_{12}*	-38	-81	137	S17 (c)
Z–H + 4-C_7H_{12}*	-62	-103	133	S17 (d)
Z–CH_3 + 1-C_7H_{12}*	-28	-93	155	S17 (e)
Z–CH_3 + 3-C_7H_{12}*	-19	-85	158	S17 (f)
Z–CH_3 + 4-C_7H_{12}*	-23	-89	157	S17 (g)
[1p-4-C_7H_{11}--H--CH_3--Z]≠	30	-16	126	S18 (e)
[1p-3-C_7H_{11}--H--CH_3--Z]≠	62	13	131	S18 (f)
[1p-2-C_7H_{11}--H--CH_3--Z]≠	71	24	127	S18 (g)
[1p-5-C_7H_{11}--H--CH_3--Z]≠	47	2	124	S18 (h)
[1p-1-C_7H_{11}--H--CH_3--Z]≠	57	13	124	S18 (i)
[1p-6-C_7H_{11}--H--CH_3--Z]≠	48	-2	133	S19 (j)
Z–H + 1-C_7H_{10}*	-72	-177	289	S17 (h)
Z–H + 2-C_7H_{10}*	-42	-148	290	S17 (i)
Z–H + 5-C_7H_{10}*	-46	-153	292	S17 (j)
Z–CH_3 + 1-C_7H_{10}*	-35	-167	316	S17 (k)
Z–CH_3 + 2-C_7H_{10}*	-27	-164	324	S17 (l)
Z–CH_3 + 5-C_7H_{10}*	-18	-150	315	S17 (m)
[1p-2-C_7H_9--H--CH_3--Z]≠	22	-94	290	S19 (k)
[1p-4-C_7H_9--H--CH_3--Z]≠	25	-86	283	S19 (l)
[1p-1-C_7H_9--H--CH_3--Z]≠	52	-62	286	S19 (m)
Z–H + C_7H_8	-189	-365	454	S17 (n)

Table S5. Adsorption Energies of C_2-C_4 alkenes in H-ZSM-5 (MFI)

State	ΔH kJ mol^{-1}	ΔG kJ mol^{-1}	ΔS J K^{-1} mol^{-1}	Structures
Ref: Z–H + C_nH_{2n} (g)	0	0	0	
Z–H + C_2H_4*	-80	17	-156	S22 (a)
Z–C_2H_5	-46	26	-116	S22 (b)
Z–H + C_3H_6*	-69	23	-147	S22 (c)
Z–1-C_3H_7	-72	36	-174	S22 (d)
Z–2-C_3H_7	-83	30	-181	S22 (e)
Z–H + C_4H_8*	-69	22	-146	S22 (f)
Z–*iso*-C_4H_9	-71	40	-180	S22 (g)
Z–*tert*-C_4H_9	-58	53	-179	S22 (h)
Z^- + *tert*-$C_4H_9^+$	-37	57	-151	S22 (i)

Table S6. Transition State Energies for alkene-mediated dehydrogenation of C_6H_{12}, C_6H_{10}, and C_6H_8 in H-ZSM-5 (MFI)

State	ΔH kJ mol^{-1}	ΔG kJ mol^{-1}	ΔS J K^{-1} mol^{-1}	Structures
Ref: Z–alkyl + C_6H_x	0	0	0	
[C_6H_{12}--C_2H_5--Z]≠	69	76	-12	S23 (a)
[C_6H_{10}--C_2H_5--Z]≠	68	74	-10	S23 (d)
[C_6H_8--C_2H_5--Z]≠	58	64	-10	S23 (g)
[C_6H_{12}--C_3H_7--Z]≠	79	80	-1	S23 (b)
[C_6H_{10}--C_3H_7--Z]≠	57	54	4	S23 (e)
[C_6H_8--C_3H_7--Z]≠	56	55	2	S23 (h)
[C_6H_{12}--C_4H_9--Z]≠	56	53	6	S23 (c)
[C_6H_{10}--C_4H_9--Z]≠	-21	-15	-10	S23 (f)
[C_6H_8--C_4H_9--Z]≠	30	5	40	S23 (g)
Ref: Z–H + alkyl* + C_6H_x(g)	0	0	0	
[C_6H_{12}--C_2H_5--Z]≠	31	131	-160	S23 (a)
[C_6H_{10}--C_2H_5--Z]≠	1	104	-165	S23 (d)
[C_6H_8--C_2H_5--Z]≠	-5	99	-167	S23 (g)
[C_6H_{12}--C_3H_7--Z]≠	48	144	-155	S23 (b)
[C_6H_{10}--C_3H_7--Z]≠	-7	89	-154	S23 (e)
[C_6H_8--C_3H_7--Z]≠	-5	92	-154	S23 (h)
[C_6H_{12}--C_4H_9--Z]≠	17	126	-175	S23 (c)
[C_6H_{10}--C_4H_9--Z]≠	-33	81	-182	S23 (f)
[C_6H_8--C_4H_9--Z]≠	-27	50	-124	S23 (g)
Ref: Z–H + alkene* + C_6H_x(g)	0	0	0	
[C_6H_{12}--C_3H_7--Z]≠	34	151	-189	S23 (b)
[C_6H_{10}--C_3H_7--Z]≠	-21	96	-187	S23 (e)
[C_6H_8--C_3H_7--Z]≠	-19	99	-188	S23 (h)
[C_6H_{12}--C_4H_9--Z]≠	28	157	-208	S23 (c)
[C_6H_{10}--C_4H_9--Z]≠	-22	112	-215	S23 (f)
[C_6H_8--C_4H_9--Z]≠	-16	82	-156	S23 (g)

S8. ***Images of Reactant, Product and Transition State Structures***

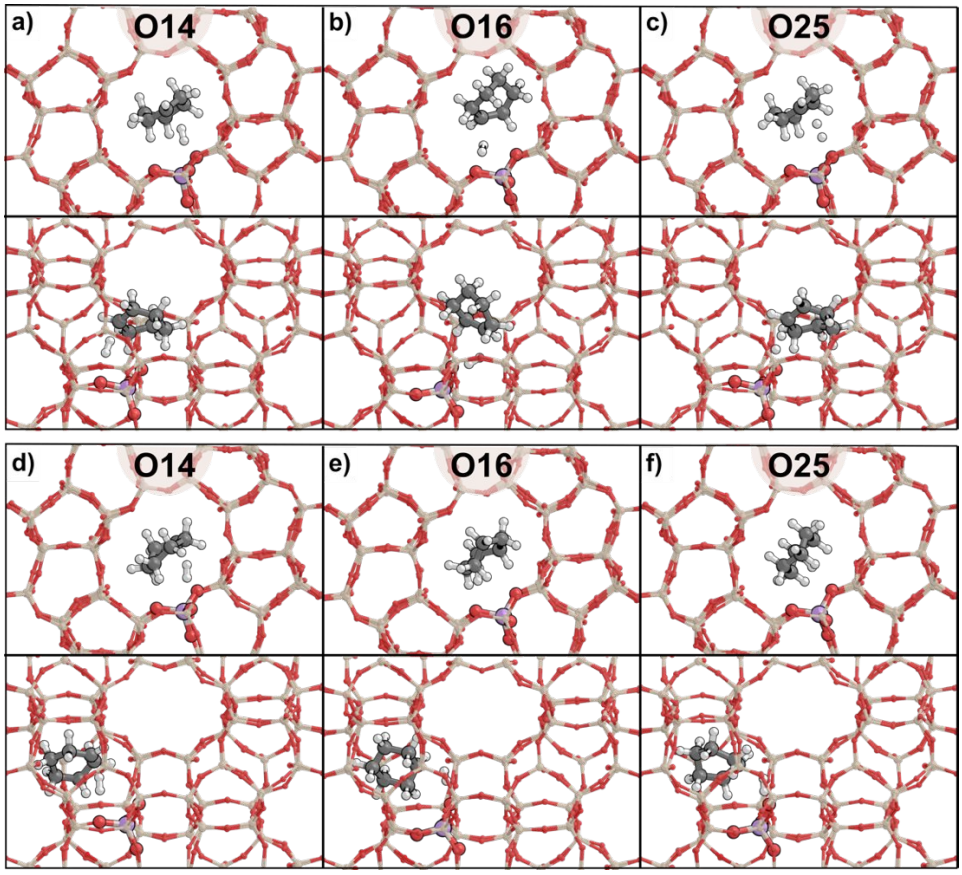

Figure S10. Transition state structures for proton-mediated dehydrogenation of cyclohexane occurring from channel intersection and straight channel.

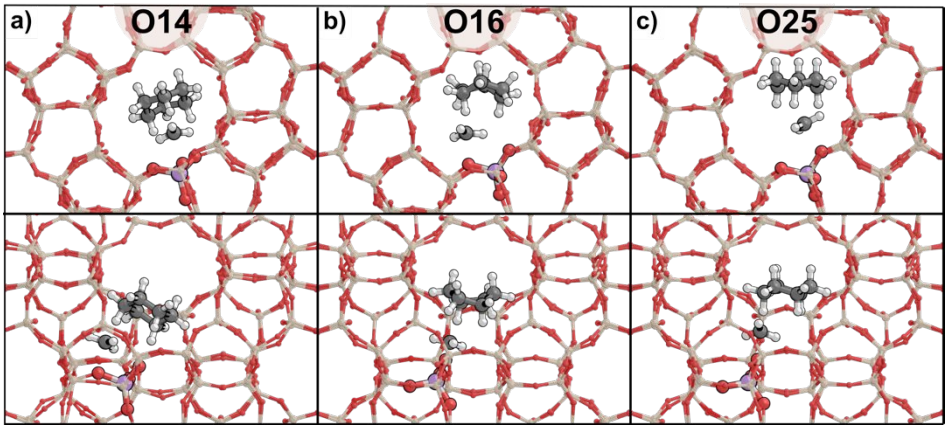

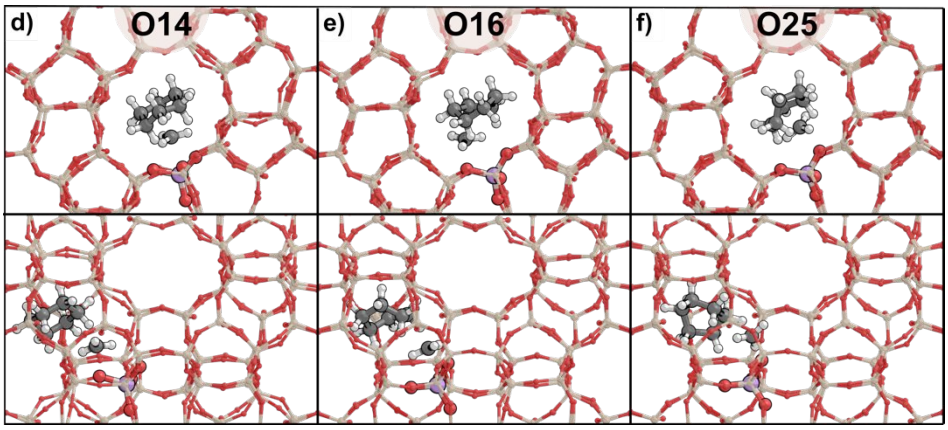

Figure S11. Transition state structures for methyl-mediated dehydrogenation of cyclohexane occurring from channel intersection and straight channel.

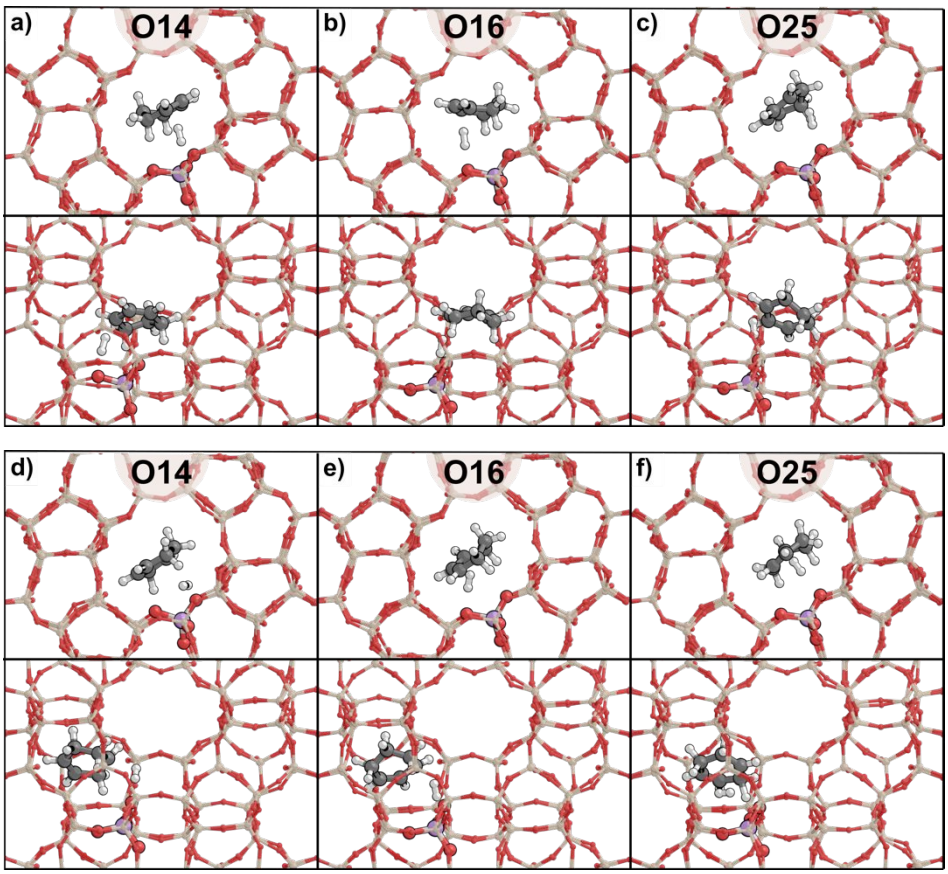

Figure S12. Transition state structures for proton-mediated dehydrogenation of cyclohexene occurring from channel intersection and straight channel.

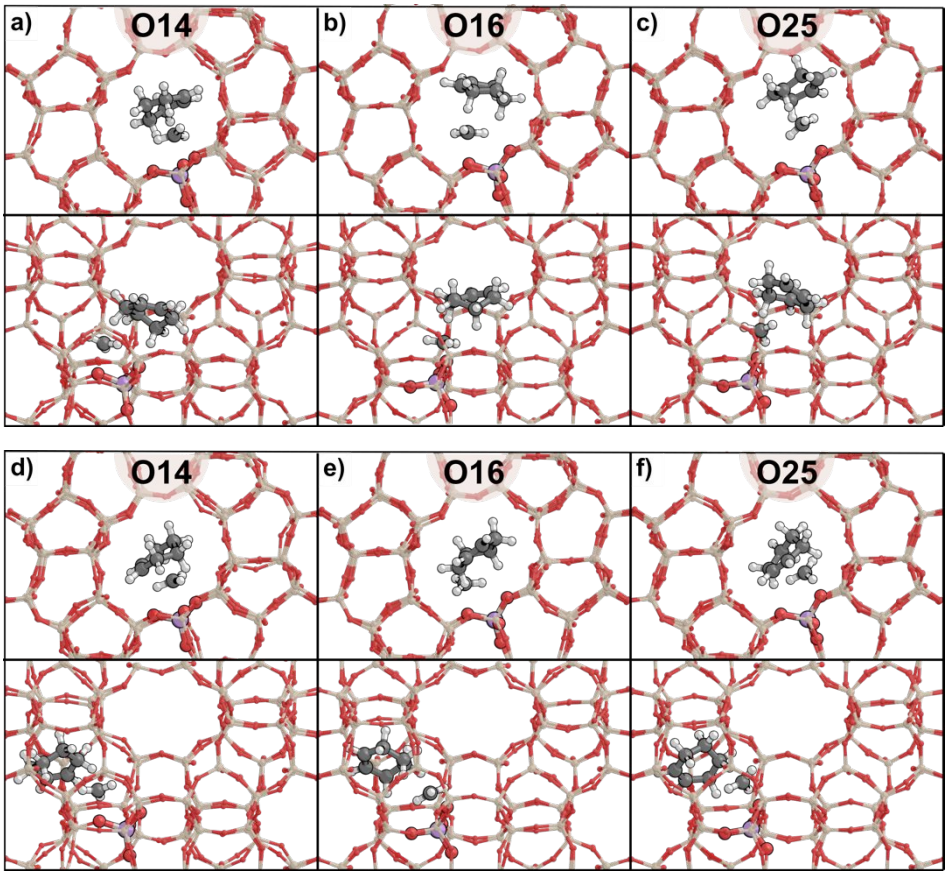

Figure S13. Transition state structures for methyl-mediated dehydrogenation of cyclohexene occurring from channel intersection and straight channel.

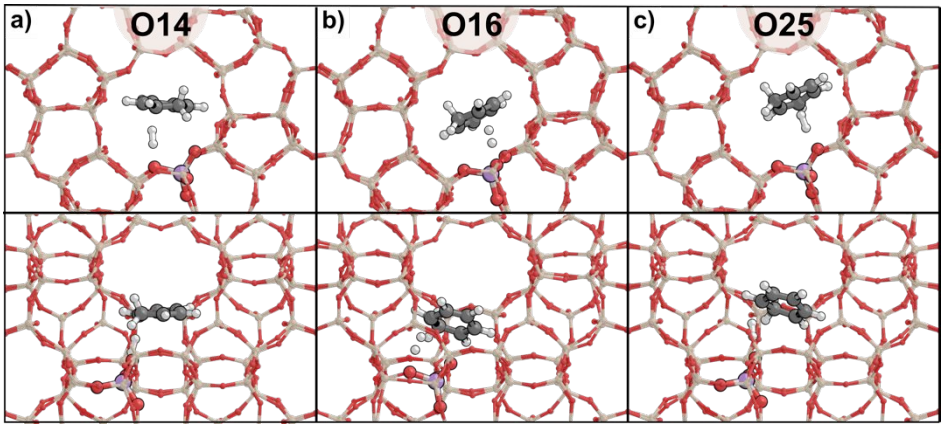

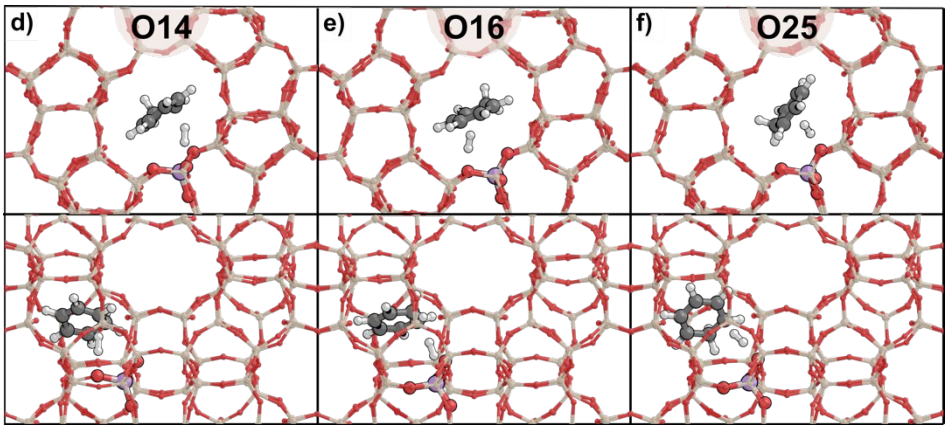

Figure S14. Transition state structures for proton-mediated dehydrogenation of cyclohexadiene occurring from channel intersection and straight channel.

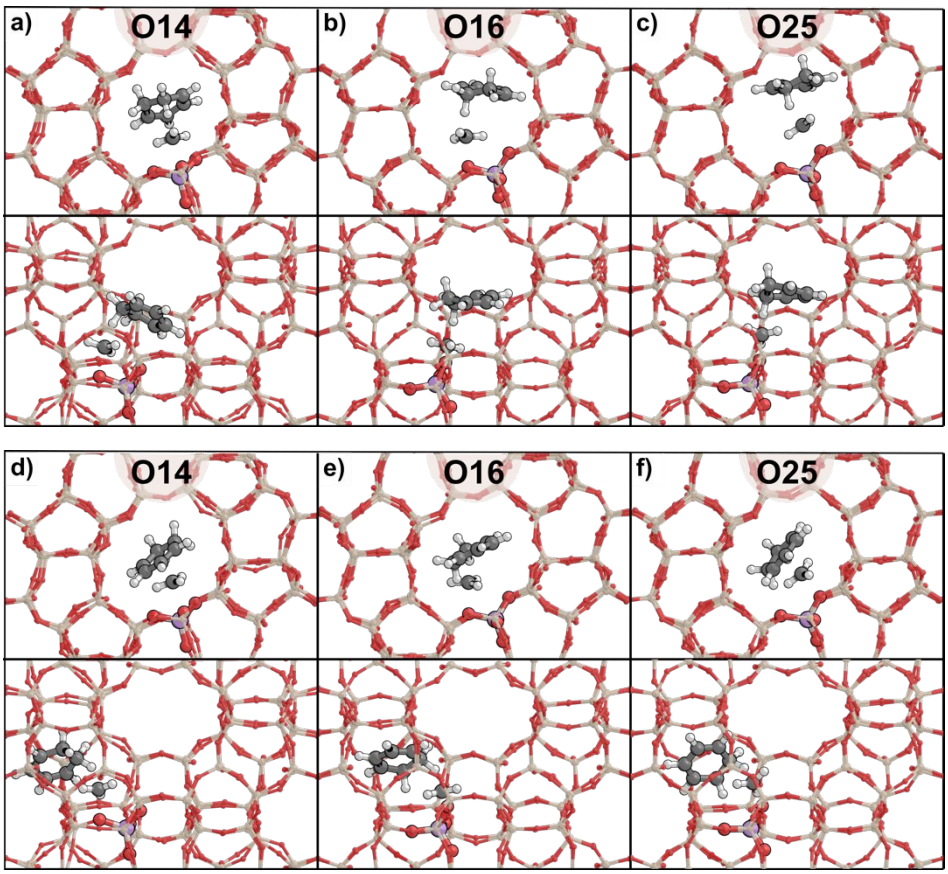

Figure S15. Transition state structures for methyl-mediated dehydrogenation of cyclohexadiene occurring from channel intersection and straight channel.

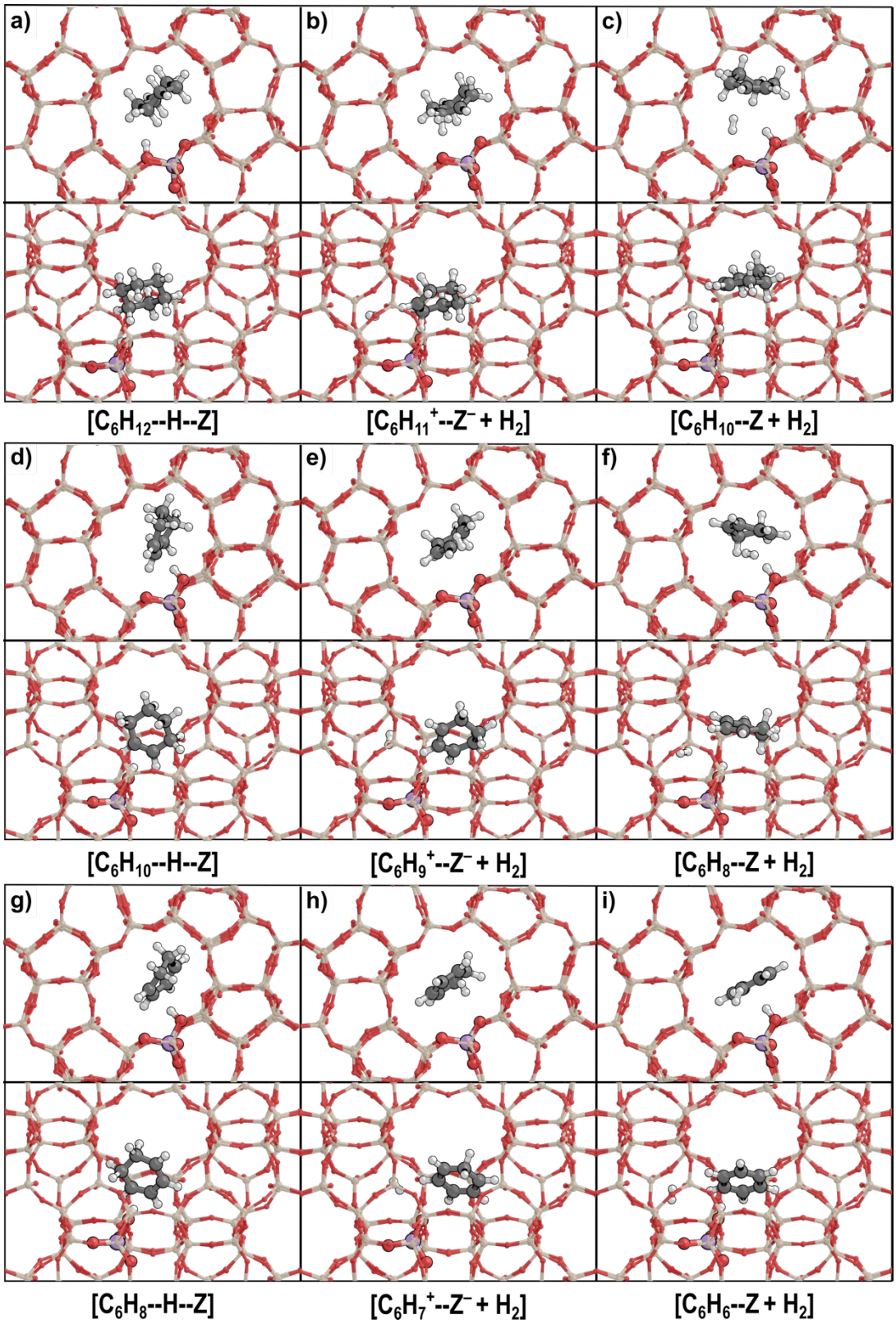

Figure S16. Reactants, carbocation intermediates, and products states for proton-mediated dehydrogenation of cyclohexane, cyclohexene, and cyclohexadiene.

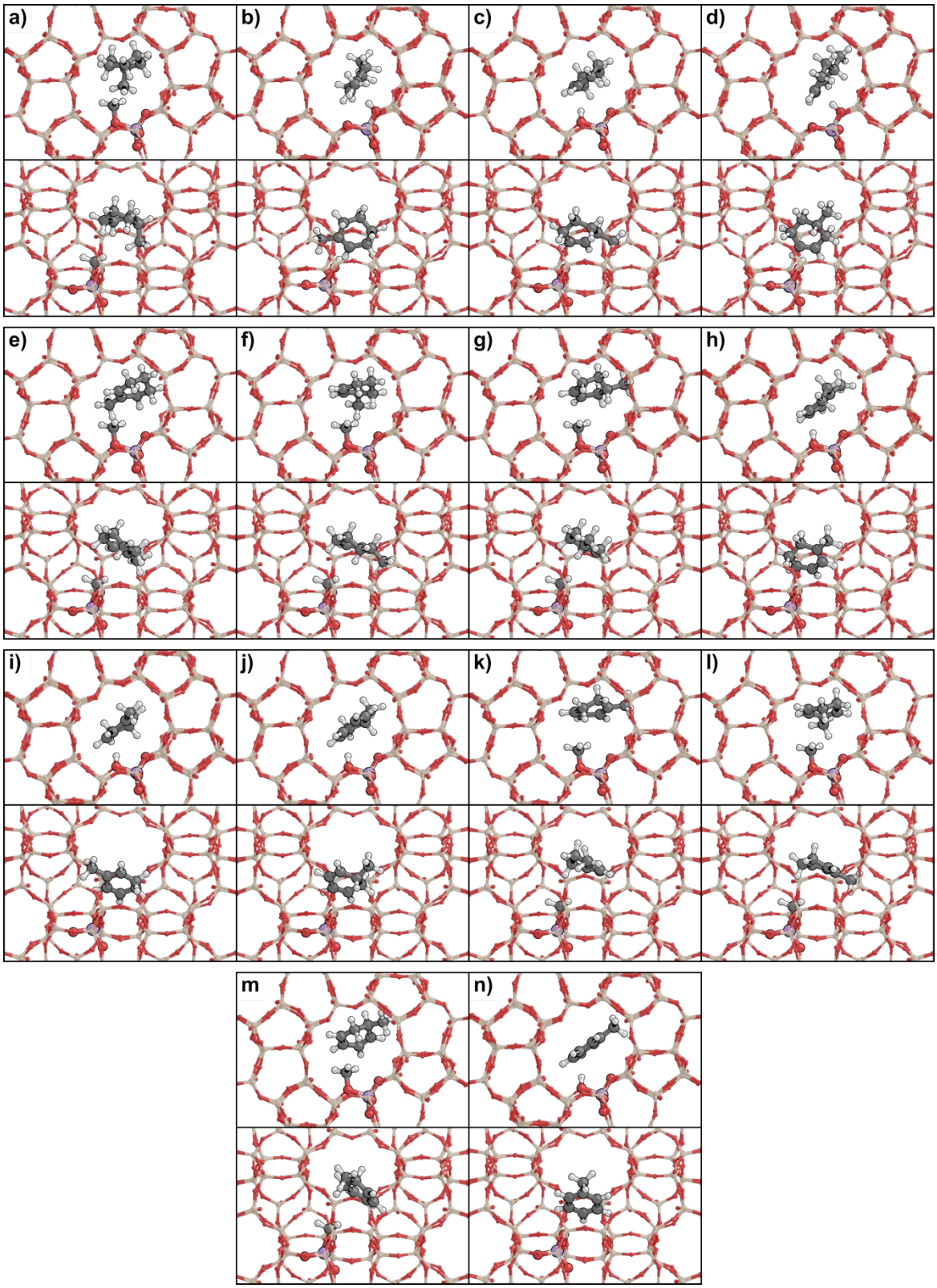

Figure S17. Reactant, intermediates, and product structures for the dehydrogenation of methyl-cyclohexane into toluene.

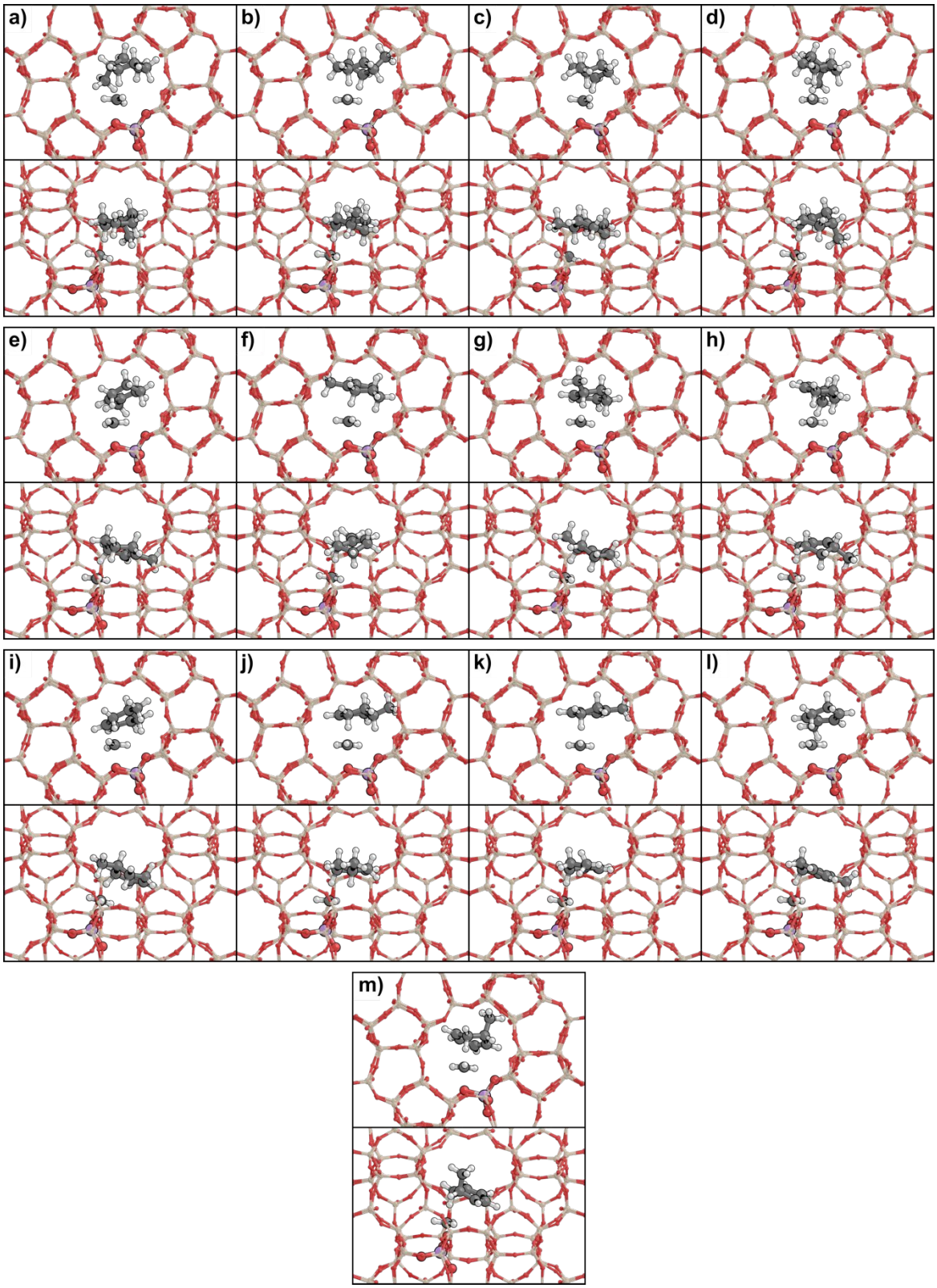

Figure S18. Transition state structures for the dehydrogenation of methyl-cyclohexane into toluene.

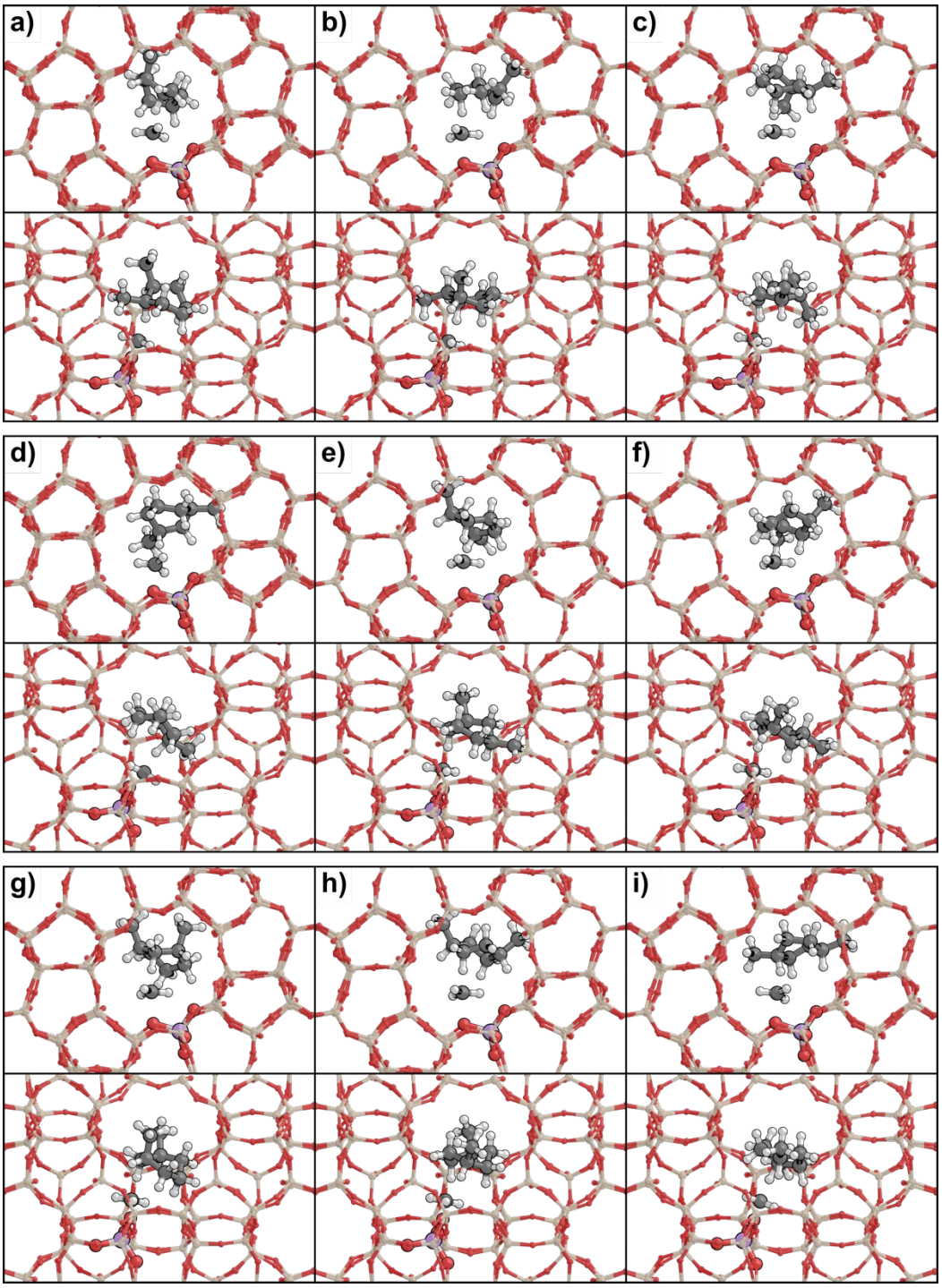

Figure S19. Transition state structures for the dehydrogenation of dimethyl-cyclohexane skeletal isomers.

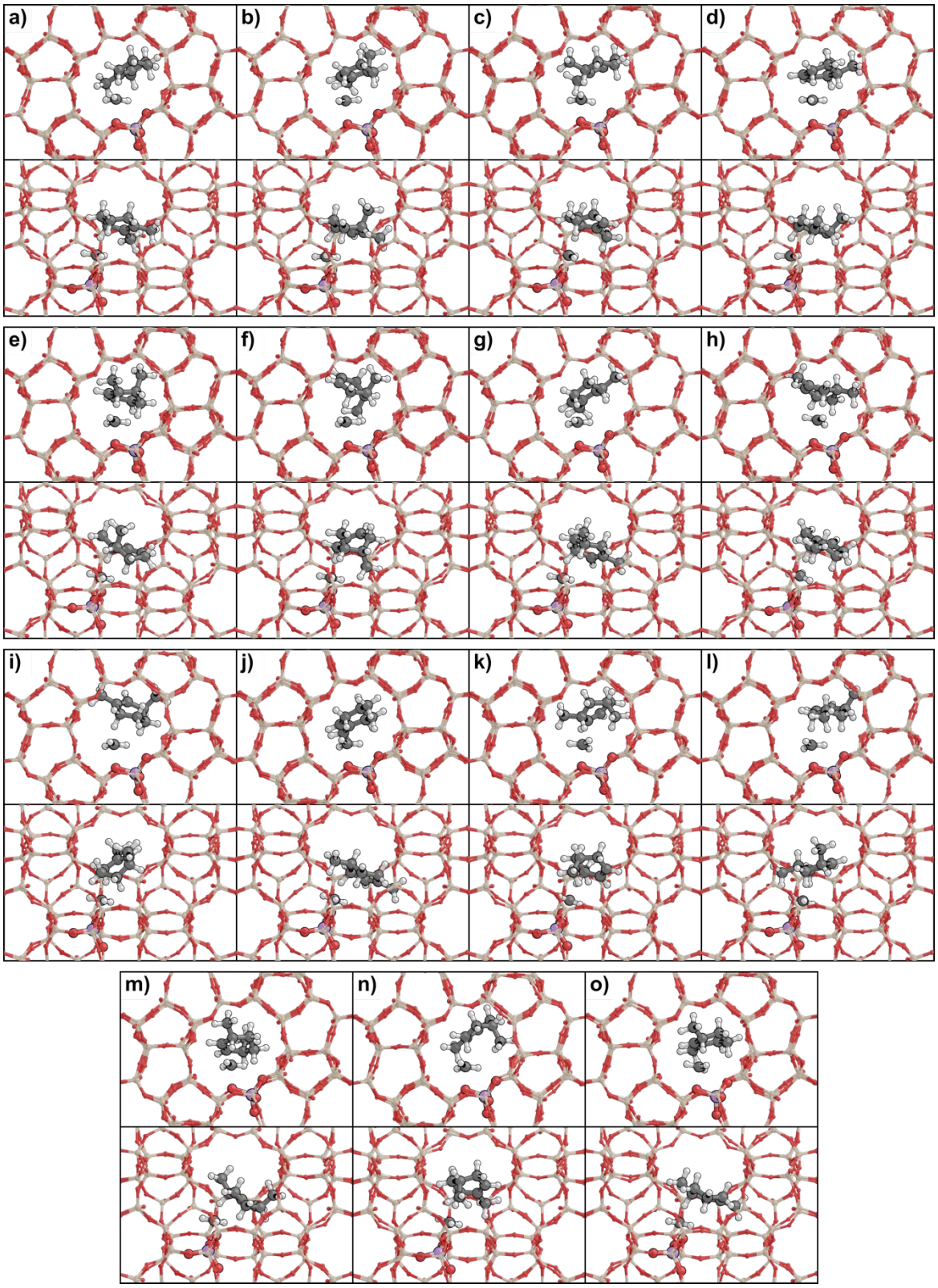

Figure S20. Transition state structures for the dehydrogenation of dimethyl-cyclohexene skeletal isomers.

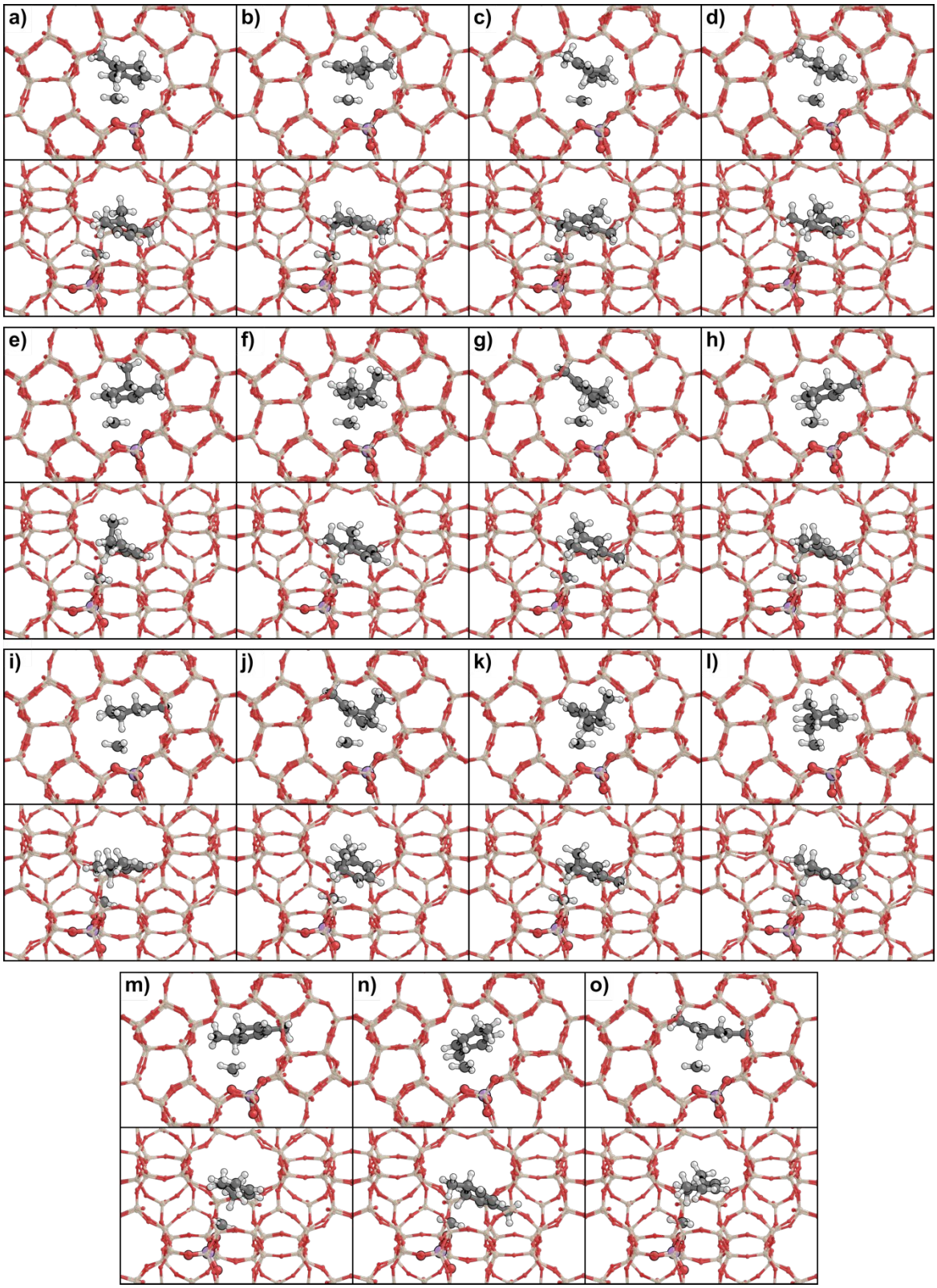

Figure S21. Transition state structures for the dehydrogenation of dimethyl-1,3-cyclohexadiene skeletal isomers.

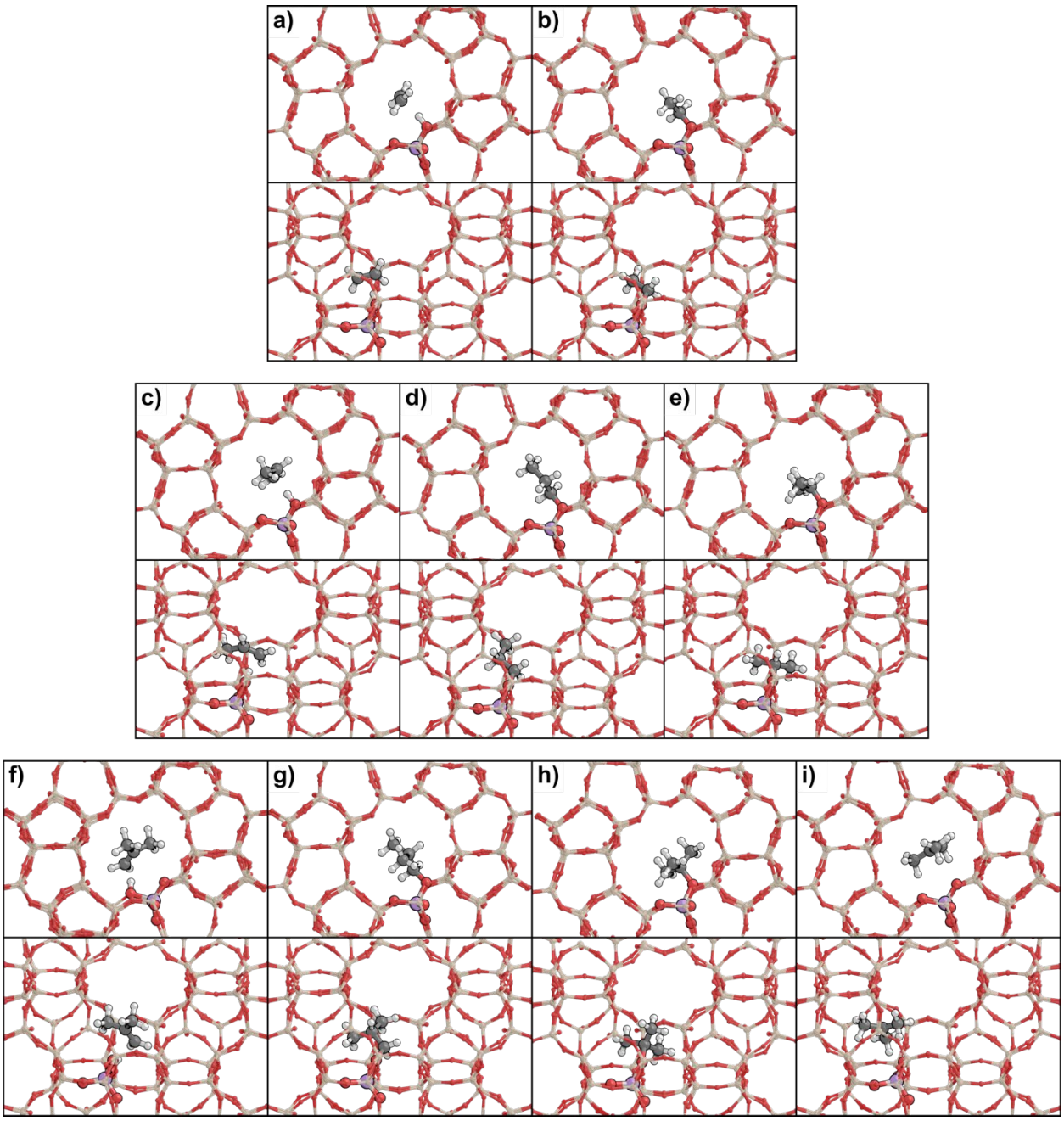

Figure S22. Binding modes structures for (a-b) ethene, (c-e) propene, and (f-i) butene.

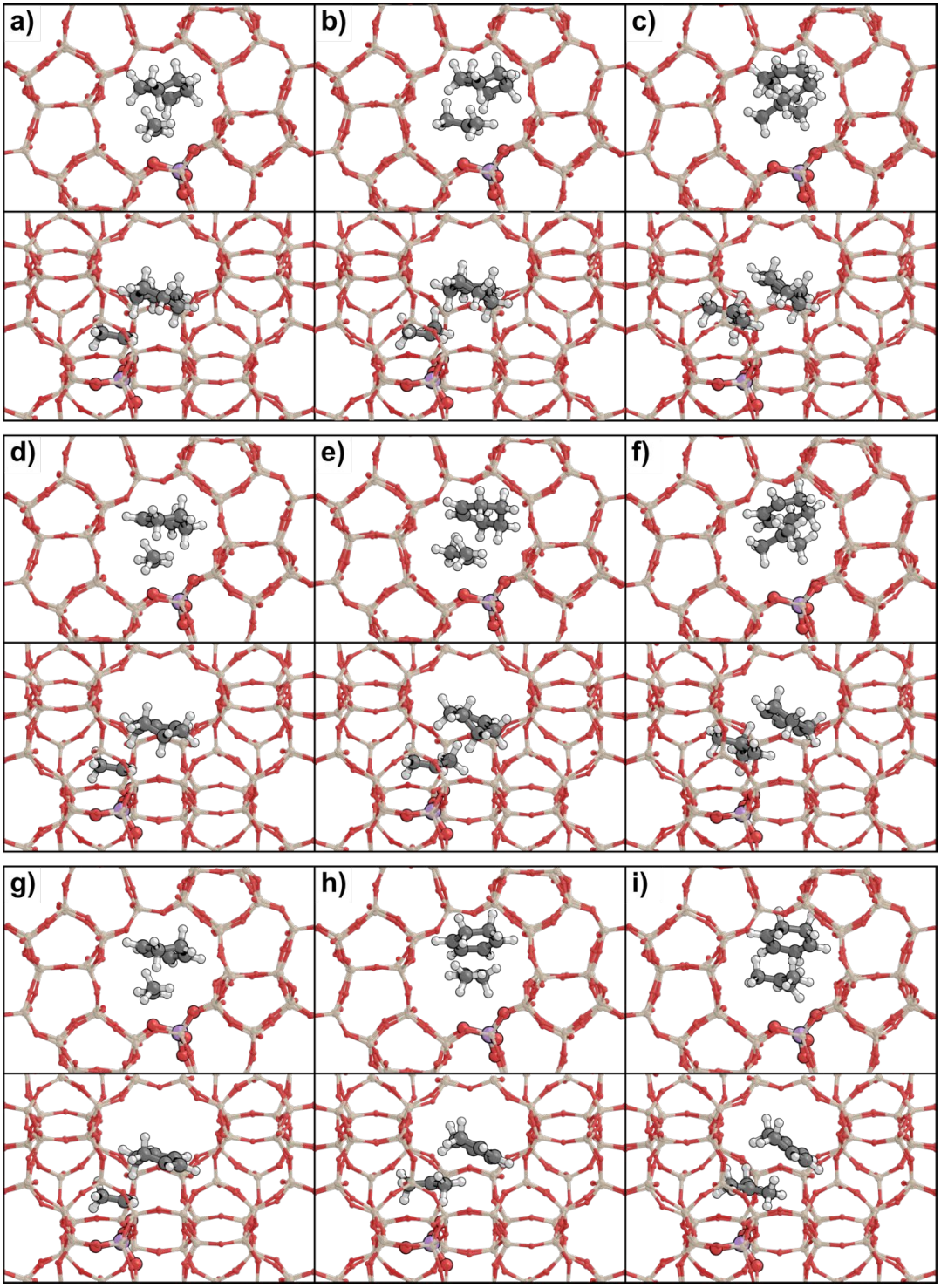

Figure S23. Transition state structures for ethyl-, 2-propyl-, and tert-butyl-mediated dehydrogenation of C_6H_{12} (a-c), C_6H_{10} (d-f), C_6H_8 (g-i), respectively.